Disorder and the optical spectroscopy of Cr^{3+}-doped glasses: I. Silicate glasses

1991 J. Phys.: Condens. Matter 3 1915

(http://iopscience.iop.org/0953-8984/3/12/022)

J. Phys.: Condens. Matter 3 (1991) 1915–1930. Printed in the UK

Disorder and the optical spectroscopy of Cr^{3+}-doped glasses: I. Silicate glasses

F Rasheed†§, K P O'Donnell†, B Henderson† and D B Hollis‡

† Department of Physics and Applied Physics, University of Strathclyde, Glasgow G4 0NG, UK

‡ Department of Physics, Paisley College of Technology, Paisley PA1 2BE, UK

Received 8 June 1990, in final form 23 October 1990

Abstract. This paper reports optical absorption and luminescence studies of Cr^{3+}-doped silicate glasses with compositions chosen to vary the octahedral crystal-field splitting at the Cr^{3+} site. The extensive site-to-site disorder in the glasses is signalled by the inhomogeneous broadening of radiative transitions and by non-exponential fluorescence decay patterns. Laser-excited luminescence shows that the octahedral crystal-field splitting Dq varies between the different sites occupied by Cr^{3+} ions. Both R-line and $^4T_2 \rightarrow {}^4A_2$ emissions are inhomogeneously broadened by site-to-site disorder. Fluorescence line narrowing (FLN) of the R line gives a particularly dramatic demonstration of the site multiplicity. Measurement of the width of the FLN component of the R line as a function of temperature has been used to probe the density of two-level vibrational systems coupled to the electronic levels of the Cr^{3+} ion.

1. Introduction

The optical absorption and luminescence properties of Cr^{3+} ions are normally interpreted in terms of crystal-field levels originating on the free-ion LS-terms of the $3d^3$ configuration. Apart from a common term, the free-ion energies are functions of inter-electron interaction (Racah) parameters B and C. The ratio C/B is about 4.0 for pure d electrons. The interaction of the 3d electrons with octahedrally disposed lattice ions is characterized by the strength Dq of the octahedral crystal field given by

$$Dq = [Ze^2/6(4\pi\varepsilon_0)](\langle r^4\rangle_{3d}/a^5) \tag{1}$$

where $\langle r^4\rangle_{3d}$ is the expectation value of the fourth power of the orbital radius of the 3d shell and a is the distance of the transition-metal ion from six nearest-neighbour ligand ions. The removal of energy degeneracy by the octahedral crystal field is represented on a Tanabe–Sugano diagram in which the energy E/B of each level is plotted as a function of Dq/B for constant ratio C/B. For the $3d^3$ configuration, only the ^4F, ^2G and ^4P levels need be considered. As figure 1 shows, the free-ion ground state ^4F splits into three crystal-field levels $^4A_2$, $^4T_2$ and $^4T_1$ in ascending order, which are classified by irreducible representations of the O_h group. The free-ion ^4P state is not split in octahedral fields and transforms as the $^4T_1$ irreducible representation of O_h. The low-lying ^2G term yields $^2A_1$, ^2E, $^2T_1$ and $^2T_2$ levels of which ^2E is lowest.

§ Permanent address: Department of Physics, Military Engineering Academy, Baghdad, Iraq.

0953-8984/91/121915 + 16 $03.50

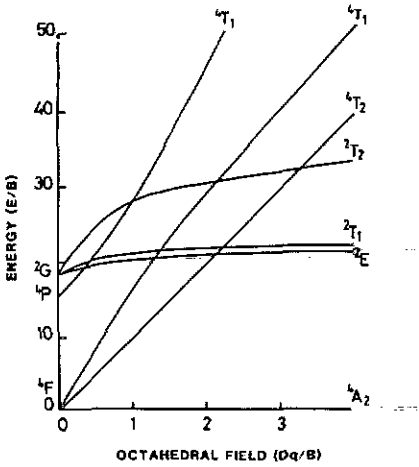

Figure 1. A Tanabe–Sugano diagram for Cr^{3+} ions in octahedral crystal fields. Values of E/B are plotted as a function of Dq/B with $C/B = 4.5$.

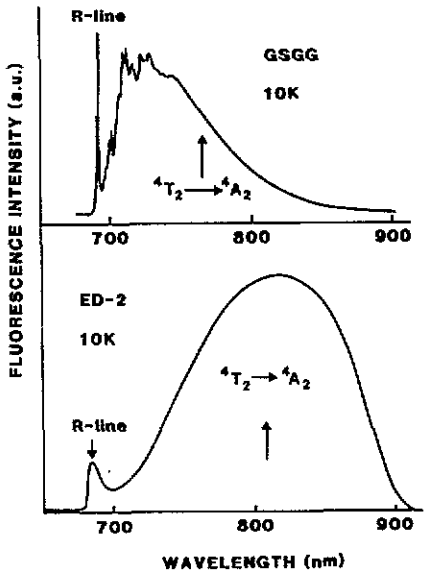

Figure 2. Photoluminescence spectra of GSGG: Cr^{3+} and ED-2: Cr^{3+} measured at 10 K, excited using the 488 nm Ar^+ laser line.

Cr^{3+} ions have strong visible absorption bands due to the spin-allowed but parity-forbidden $^4A_2 \rightarrow {}^4T_2$ and $^4A_2 \rightarrow {}^4T_1$ transitions. The widths of these bands imply strong electronic coupling to vibrations of the local environment. Since the spin- and parity-forbidden $^4A_2 \rightarrow {}^2E$ and $^4A_2 \rightarrow {}^2T_1$ absorptions are only weakly coupled to the vibrational spectrum, they appear as weak narrow lines superimposed on the $^4A_2 \rightarrow {}^4T_2$ absorptions band. The fluorescence spectrum depends upon the value of Dq/B. For ruby Al_2O_3: Cr^{3+}, $Dq/B = 2.8$ so that ^2E lies below $^4T_2$ (figure 1). The fluorescence spectrum reveals the presence of the very sharp R lines. In contrast, Cr^{3+} ions occupying low-field sites, in which $^4T_2$ lies below ^2E, emit into the broad-band $^4T_2 \rightarrow {}^4A_2$ transition. The examples given in figure 2 are for Cr^{3+} ions in crystalline $Gd_3Sc_2Ga_3O_{12}$ (GSGG) and in a commercial silicate glass (ED-2). Both are disordered solids. In GSGG the disorder is limited to three or four distinct sites (Struve and Huber 1985, Boulon *et al* 1988, Monteil *et al* 1988, Healey *et al* 1989, Marshall *et al* 1990); the emission spectrum at 4 K comprises R lines with vibronic structure (i.e. $^2E \rightarrow {}^4A_2$ transition) overlapping the short-wavelength tail of broad-band $^4T_2 \rightarrow {}^4A_2$ transition near 700 nm. In silicate glasses, discussed in this paper, multi-site distortions give rise to Dq/B-values ranging from 1.98 to 2.25. Greatest fluorescence intensity is observed in the $^4T_2 \rightarrow {}^4A_2$ broad-band fluorescence, which is shifted to longer wavelengths relative to GSGG because most Cr^{3+} ions occupy weak-field sites. The R line is also very much broader than for GSGG and is accompanied by a rather weak vibronic sideband.

2. Structure of silicate glasses

It is hard to incorporate Cr^{3+} in vitreous silica. Such few results as exist indicate a range of ligand fields lower than in ruby ($Dq/B \simeq 2.8$), but high enough to give a strong ^2E

Table 1. Compositions of Cr^{3+} silicate glasses.

	Amount (mol%)										
Glass	SiO_2	Li_2O	Na_2O	K_2O	CaO	PbO	Al_2O_3	As_2O_3	B_2O_3	Cr_2O_3	CeO_2
ED-2	60.0	27.3	—	—	10.0	—	2.5	—	—	0.05	0.15
G8035	68.59	15.74	—	—	10.73	—	4.91	—	—	0.03	—
SLS7b/7	69.68	—	20.63	—	9.38	—	—	0.28	—	0.02	—
SLS7b/4	73.61	—	—	12.38	—	12.38	—	0.31	1.28	0.05	—

Table 2. Polymeric constitution of silicate glasses.

	Amount (mol%)			
	ED-2	G8035	SLS7b/7	SLS7b/4
SiO_2 network	50	41	41	67
SiO_4^{4-} tetrahedra	40	30	30	15
$Si_2O_7^{6-}$ sheets or rings	10	16	16	8
$Si_3O_{11}^{8-}$ rings	—	13	13	10

emission. The conversion of silica to its glassy form leads to a randomization of the quartz network, obtained by a dissymetric rotation of the $(SiO_4)^{2-}$ tetrahedra relative to one another; although the Si–O bond lengths remain almost unchanged, the O–Si–O bond angles range over values the exact spread of which is controversial (Barrer and Vaughan 1967, Shackelford and Masaryk 1978, Shelby 1979, Mitra and Hockney 1980, Howitt and Elfresh 1982, Siefert *et al* 1983). The Si–O bonds are essentially covalent, and both crystalline and vitreous SiO_2 approximate to a covalently bonded continuous three-dimensional network. This paper is concerned with the optical spectroscopy of Cr^{3+} ions in a range of silicate glasses, the compositions of which are given in table 1. Silicate glasses have wide ranges of composition in which modifiers such as Na_2O are added to break up the random network of SiO_2 tetrahedra, and stabilizers such as Al_2O_3 or B_2O_3 prevent crystallization. For example, Si–O–Si bonds in the G8035 glass (table 1) are broken and replaced by $Si–O^-–Ca^{2+}–O^-–Si$ and similar linkages. Network modifiers are especially important in Cr^{3+}-doped glasses since in breaking up the SiO_2 network they enable the $3d^3$ ion to occupy 'octahedrally' coordinated sites. With addition of up to about 10% R'_2O or $R''O$, the system consists of a 'damaged' three-dimensional network in which the modifiers occupy pre-existing vacancies (Lacy 1955). At greater modifier concentrations, as in the glasses studied here, distinct entities such as sheets and rings appear (Balta and Balta 1976, Paul 1982).

Yang and Chen (1989) have discussed probable polymeric entities in silicate glasses; the compositions in table 1, which approximate those of Yang and Chen, have the polymeric contents given in table 2. Evidently, as the silica content increases, the amount of undamaged silica network and sheets or rings increase whereas that part of the silica which has reacted with alkali ions changes so that isolated SiO_4^{4-} tetrahedra become less common. In addition, modifiers distend the network, altering the oxygen packing density

partly by virtue of their size and resultant polarizing power Ze^2/r and partly through the degree of network disruption, which depends on the relative number of modifier ions (Lacy 1955). Cr^{3+} ions must reside in the reacted part of the network, where they are strongly affected by the type of modifier cation and polymeric group. The ligand field is determined by the modifier type, because of the resultant compaction or distention of that fraction of the SiO_2 which has reacted with the modifying cations (Lacy 1955, Imbusch *et al* 1990). In consequence, modifier ions destroy the long-range periodicity, resulting in open structures with long distances between Cr^{3+} ions and ligands. Furthermore large modifiers occupy large spaces with high coordination, expanding the whole network. Since the octahedral field strength Dq varies as a^{-5}, modifier ions require that Cr^{3+} ions find lower ligand fields. That the Cr^{3+} impurities occupy distorted 'octahedral' sites is indicated by electron spin resonance (ESR) spectra. Crystal-field splittings are larger in the orbitally degenerate excited states than in the ground state and the effects of disorder are more extensive in optical spectra than in ground-state ESR spectra. The experimental results reported here are shown to be in accord with these general concepts. However, as discussed below, the luminescence output is determined not only by the glass composition but also by excitation wavelength and the time scale of the detection process. The rich variety of spectral features discussed below showed that the Cr^{3+} ion is a valuable probe for the structure of glasses.

3. Experimental techniques

This paper discusses the optical properties of Cr^{3+}-doped silicate glasses containing some 60–78 wt% SiO_2 and network modifiers Li_2O, Na_2O and K_2O which differ in both content (16–32 wt%) and ionic radii (table 1). The samples SLS7b/4 and SLS7b/7 were prepared by mixing Loch Aline sand with sodium carbonate and calcium carbonate in the correct proportions to give the glass with the appropriate (approximate) molar composition. The carbonates were of Analar grade, and the main impurity was 0.04 wt% Fe_2O_3 in the sand. All other impurities were negligible. The lead crystal glass SLS7b/4 was melted in a mullite crucible at 1450 °C for 7 h in a gas–air furnace set to an oxidizing flame. Then discs were poured into steel moulds and annealed at 550 °C for 0.5 h before being allowed to cool to room temperature for 18 h. The soda–lime glass SLS7b/7 was prepared in a similar fashion, except that the crucible was of crystallized alumina and that the gas–air flame was reducing. These two changes ensured that nearly all the chromium would be maintained in the trivalent state. Leaching of the mullite crucible by the alkalis in the batch caused iron contamination in SLS7b/4. Sample G8035 was prepared by Dr S E Stokowski at Lawrence Livermore Laboratory and ED-2 was a commercial glass provided by Professor G F Imbusch of University College, Galway. The compositions of all these glasses are given in table 1.

ESR spectra were measured at X band (9.5 GHz) and Q band (35 GHz) at room temperature. Samples used for optical absorption measurements were cut and polished to dimensions of 1 mm × 5 mm × 7 mm. The optical absorption coefficient was measured at 77 and 300 K in the wavelength range 250–900 nm. Laser-excited fluorescence was measured from glass samples cut and polished to dimensions of 1 mm × 2 mm × 5 mm using an Ar^+ laser or a dye laser pumped using the all-lines output from the same Ar^+ laser. Low optical pump power was used to minimize thermal gradients in the sample. The fluorescence was focused onto the entry slit of a 1 m scanning monochromator and detected at the exit slit using a GaAs or cooled Si photodetector.

The excitation was mechanically chopped at frequencies ranging from 10 Hz to 3 kHz; the mechanical chopper also provided a reference signal for the phase-sensitive electronics, which allowed for the detection, collection and analysis of data using a microcomputer. The $^4T_2 \rightarrow {}^4A_2$ transition, being spin allowed, normally has a much shorter lifetime than the spin-forbidden $^2E \rightarrow {}^4A_2$ emission. The two spectra overlap to some extent in the range 690–715 nm. Time resolution of overlapping fluorescence spectra having different decay times was achieved by connecting a chopped-signal integrator to the output of the photodetector to process the low-level signal detected when chopped laser light illuminates the sample. The synchronizing reference signal from the chopper was delayed and stretched to define two time windows: one for the signal and the other for the reference zero. The signal voltages during these two time windows were separately integrated and then subtracted to give a steady-state output signal. The ^2E and $^4T_2$ emission signals were separated by setting the signal window to the start of the decay and the zero window at the end part of the decay. Only the longer-lived component was then observed. The temporal evolution of these changes was then measured using a boxcar integrator. A series of spectra were recorded after different time delays; after a time delay of about 2 ms the fast $^4T_2$ emission had completely decayed, allowing the R-line emission to be detected at longer delays. Alternatively, phase-sensitive detection enables separate R-line and broad-band $^4T_2 \rightarrow {}^4A_2$ spectra to be recorded (Engstrom and Mollenauer 1973).

The inhomogeneous broadening of the R line was probed using fluorescence line narrowing (FLN). A narrow laser line was used to pump within the inhomogeneous linewidth Γ_{inh}, exciting only that subset of ions with energy levels spanning the bandwidth Γ_L of the laser. The fluorescence linewidth when these centres re-radiate approached the homogeneous width Γ_h, which is much narrower than the inhomogeneous width. In fact the width Γ of the FLN component is a convolution of laser linewidth and twice the homogeneous linewidth Γ_h, i.e.

$$\Gamma(T) = \Gamma_L + 2\Gamma_h(T). \tag{2}$$

the T in parentheses indicates that Γ_h and therefore Γ are temperature dependent (Kushida and Takushi 1975). A single-mode ring dye laser was used to excite the fluorescence. For tunability over the broad R line of these Cr^{3+}-doped glasses the dye used was DCM, and Γ_L was about 500 kHz. To extract the weak FLN signal in the presence of strong scattered laser light the excitation light was chopped; the emission was also chopped to prevent scattered laser light from falling on the window of the phototube in a short period (about 10 μs) after the excitation pulse. The FLN signal was detected using different slots in the chopper wheel using a relatively long time window. The measured FLN width was then of the order of 1 GHz at low temperatures (about 10 K). The temperature-dependent variations $\Gamma_h(T)$ were measured for ED-2, G8035 and SLS7b7 over the temperature range 10–130 K.

4. Results and discussion

4.1. ESR spectra

This paper is primarily concerned with the optical properties of four Cr^{3+}-doped silicate glasses (table 1). That the crystal-field sites occupied by Cr^{3+} ions in these glasses are approximately octahedral is confirmed by ESR spectra at X band and Q band (35 GHz),

which reveal in each case a single asymmetric line due to $\Delta M_s = +\frac{1}{2} \leftrightarrow -\frac{1}{2}$ transitions with g-values in the range 1.98–1.99. The ESR lines are inhomogeneously broadened ($\Delta H \simeq 10$ mT) by Cr^{3+} occupying many different sites where distortions from octahedral symmetry result in **g**-tensor anisotropy and fine-structure splittings. Typical half-widths are of order $\Gamma_{inh} = 10$ mT. Such linewidths are characteristic of small g-shifts (about ± 0.02) and energy splittings between the $\pm\frac{3}{2}$ and $\pm\frac{1}{2}$ spin states in zero magnetic field of about 0.05–0.06 cm^{-1} (Henderson and Hall 1967). Such splittings are consistent with Cr^{3+} ions occupying weakly perturbed octahedral sites (Henderson and Wertz 1978). This is not surprising since the $3d^3$ configuration has maximum stabilization energy in octahedral symmetry.

4.2. Absorption measurements

Typical optical absorption spectra measured at 300 K are shown in figure 3; little difference is observed at 77 K. The two broad bands are due to absorption transitions from the $^4A_2$ ground state of Cr^{3+} ions to the $^4T_2$ and $^4T_1$ excited states. Weak lines overlapping the $^4A_2 \rightarrow {}^4T_2$ absorption band due to transitions to the $^2T_1$ and ^2E states are much broader than the corresponding features in oxide crystals (Henderson and Imbusch 1989, ch 9). The spectrum from a thin sample of the ED-2 glass (figure 2(b)) shows the strong charge transfer band at about 360 nm due to Cr^{6+} ions. Since Cr^{6+} absorbs in the UV below 400 nm, excitation of photoluminescence from Cr^{3+} ions alone requires that visible sources are used. The experimental energies of the absorption bands (table 3) may be used to determine the strength Dq of the octahedral crystal field and the Racah parameters B and C (Sugano *et al* 1970). In octahedral symmetry the energy difference between $^4A_2$ and $^4T_2$ states is equal to $10Dq$, which is measured from the peak $h\nu_1$ of the $^4A_2 \rightarrow {}^4T_2$ aborption band. The value of B, determined from the energy separation Δ between the $^4A_2 \rightarrow {}^4T_2$ and $^4A_2 \rightarrow {}^4T_1$ absorption peaks, is given by

$$B = \tfrac{1}{2}(2\nu_1 - \nu_2)\Delta/(9\nu_1 - 5\nu_2) \tag{3}$$

ν_2 being the energy value at the peak of the $^4A_2$–$^4T_1$ absorption band. The C-parameter is calculated from the position of the $^4A_2 \rightarrow {}^2E$ absorption peak using the equation

$$E(^2E)/B = 3.05(C/B) + 7.9 - 1.8(B/Dq) \tag{4}$$

which is accurate to about 5% for Dq/B and C/B in the ranges 1.5–3.5 and 3–5, respectively. The values of Dq/B in table 3 indicate that Cr^{3+} ions occupy weak-field sites. Since equations (2)–(4) do not allow for distortions from octahedral symmetry, the tabulation represents average values.

4.3. Steady-state luminescence

Photoluminescence spectra of ED-2, SLS7b7 and SLS7b/4 glasses are shown in figure 4: the shape of the emission spectrum of G8035 is much like that of the ED-2 glass (figure 4(a)). The measurements were made at $T = 10$ K with excitation wavelengths at the peak of the $^4A_2 \rightarrow {}^4T_2$ aborption band. The broad line near 695 nm is close to the peak in the $^4A_2 \rightarrow {}^2E$ absorption line, confirming it to be R line, inhomogeneously broadened by the multiple-site occupancy by Cr^{3+} ions in ED-2, G8035 and SLS7b/7 glasses. R-line emission is not observed from the SLS7b/4 glass (figure 4(c)) because in this glass Cr^{3+} ions occupy low-field sites and emit into the broad $^4T_2 \rightarrow {}^4A_2$ band with peak near 895 nm. The different intensities of the $^4T_2$ and ^2E emission peaks in these spectra reflect

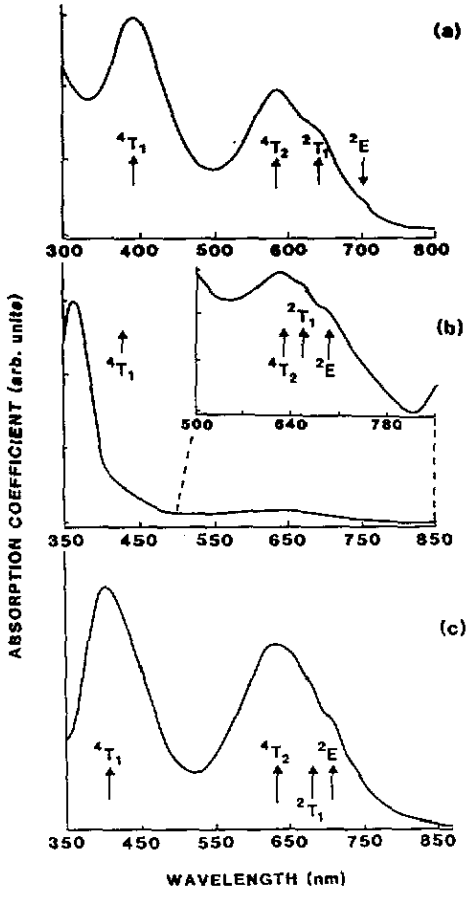

Figure 3. Optical absorption spectra of Cr^{3+} ions in (*a*) the SLS7b4, (*b*) ED-2 and (*c*) G8035 glasses. In the inset to (*b*) a sample thickness of only 0.01 mm was used. The spectra were recorded at $T = 300$ K.

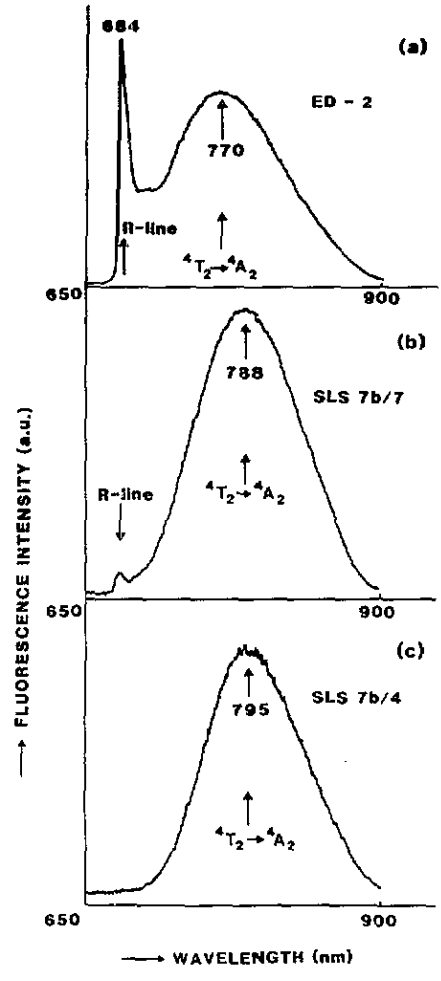

Figure 4. Typical photoluminescence spectra of Cr^{3+}-doped silicate glasses measured at 10 K: (*a*) the spectrum from the ED-2 glass excited at $\lambda = 582$ nm; (*b*) SLS7b/7 excited at 591 nm; (*c*) SLS7b/4 glass excited at 594 nm.

Table 3. Crystal-field terms of Cr^{3+} ions in glasses. All energy levels assume that the ground state $^4A_2$ is at the zero energy.

	Energy level (cm^{-1})						
	^2E	$^2T_1$	$^4T_2$	$^4T_1$	B	C	Dq/B
SLS7b/4	14616	15683	15106	22222	763.1	2595	1.98
SLS7b/7	14616	15697	15552	22727	758.5	2609	2.05
G8035	14641	15898	15723	22779	741.5	3085	2.12
ED-2	14594	15389	15904	22989	739.7	3076	2.15

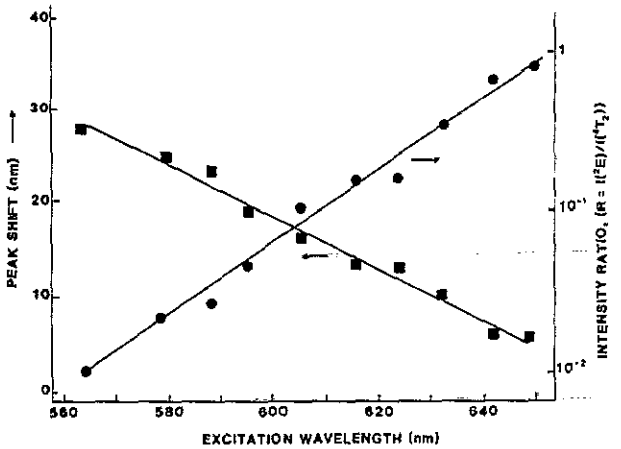

Figure 5. Effect of excitation wavelength on the emission bandshape for the ED-2 glass at 10 K.

the different (average) values of the octahedral crystal field in the silicate glasses. In fact the values of Dq/B determined from the absorption spectra (table 3) imply that these silicate glasses provide exclusively low-field sites. However, as anticipated from section 2 the larger modifier ions (Pb^{2+} and K^+) result in more open structures (e.g. for SLS7b/4), lowering the oxygen packing density and increasing the predominance of low-field sites. The ED-2 and G8035 glasses contain smaller modifier cations (Ca^{2+} and Li^+) and have larger average values of Dq/B and a significant proportion of high crystal-field sites where emission is via the broad-line $^2E \rightarrow {}^4A_2$ transition.

Comparison of figure 2 and figure 4(*a*) shows that the relative intensities of emission from the ^2E and $^4T_2$ states in the ED-2 glass are different because of the extensive inhomogeneous broadening of spectra in glasses relative to crystals. Laser radiation at 488 nm (figure 2) excites absorption transitions in the long-wavelength tail of the $^4A_2 \rightarrow {}^4T_1$ band of (mainly) low-field sites whereas laser radiation of 582 nm in the $^4A_2 \rightarrow {}^4T_2$ band (figure 4(*a*)) excites both low-field and high-field sites. These laser excitation studies provide an indelible signature of the effects of inhomogeneous broadening. Figure 1 shows that the energy of the ^2E state varies very little with Dq/B compared with the $^4T_2$ level. As discussed in section 4.5, selective excitation in the $^4A_2 \rightarrow {}^2E$ absorption results in relatively small shifts (3–4 nm) in the position of the R line. In contrast, narrow-band excitation in the $^4A_2 \rightarrow {}^4T_2$ absorption band leads to large shifts (30–40 nm) in the peak of the $^4T_2 \rightarrow {}^4A_2$ emission, which are linear with the excitation wavelength in the $^4A_2 \rightarrow {}^4T_2$ absorption band between 560 and 650 nm. Furthermore, as the excitation wavelength is increased over this same range, the intensity ratio $R = I(^2E)/I(^4T_2)$ decreases linearly with increasing excitation wavelength. Similar behaviour is observed in the other glasses. The trends shown in figure 5 for excitation wavelengths in the $^4A_2 \rightarrow {}^4T_2$ absorption bands are due to the Cr^{3+} site multiplicity in which different numbers of ions in the different sites are excited at each wavelength. Short-wavelength radiation predominantly excites Cr^{3+} ions in high-field sites, whereas longer-wavelength radiation excites mainly ions in low-field sites.

The effects of inhomogeneous broadening on the spectra of the different glasses are shown in figure 6, these results being obtained by excitation at the peak of the $^4A_2 \rightarrow {}^4T_2$

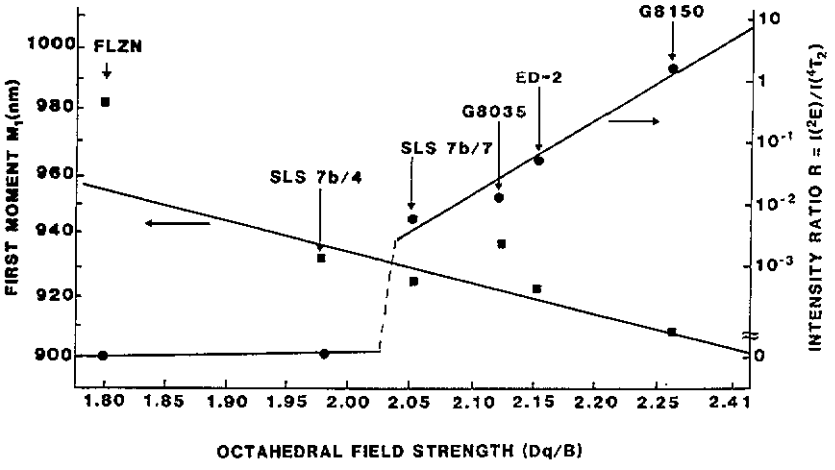

Figure 6. Variation in the intensity ratio $R = I(^2E)/I(^4T_2)$ and the first-central moment M_1 of the broad band peak as a function of the average value of Dq for the four silicate glasses. For purposes of comparison, data for a low-field fluoride glass (FLZN) and a high-field tellurite glass (G8150) are also shown. In each case the spectrum was excited close to the peak of the $^4A_2 \rightarrow {}^4T_2$ absorption band.

band at a low temperature (T= 10 K). Apparently the peak wavelength of the $^4T_2 \rightarrow {}^4A_2$ emission band undergoes almost linear shifts to longer wavelengths as the average value of Dq/B increases. The value of $R = I(^2E)/I(^4T_2)$ is essentially zero up to $Dq/B \simeq 2.05$, showing that in such glasses all Cr^{3+} ions occupy low-crystal-field sites. Above Dq/B = 2.05 the value of R increases linearly with increasing Dq/B, because at higher average Dq-values more Cr^{3+} ions occupy high-field sites. The full width of the R line implies, using equation (3), Dq/B values ranging by ± 0.06 about the average value. The data in figures 5 and 6 show that the experimental lineshapes (figure 4) are a complex convolution of individual lineshapes for which the values of R decrease as Dq/B decreases. The discontinuity in the intensity ratio for $Dq/B \simeq 2.05$ occurs because glasses such as SLS7b/4 provide only low-field sites for the Cr^{3+} ions. Indeed, since $Dq/B < 2.3$ for all four glasses, they would normally be regarded as low-field glasses in which the $^4T_2$ is energetically lower than ^2E state. Apparently, SLS7b/7, G8035 and ED-2 provide sites in which ^2E and $^4T_2$ are close together. The effects of spin–orbit coupling and electron–vibrational interaction then admix ^2E and $^4T_2$ states together with the result that the fluorescence band shape is always a mélange of the R-line and broad-band components (Yamaga *et al* 1989, 1990). The relative amounts of R line and broad band vary as the average value of Dq/B because this determines the energy splitting $\Delta E = E(^4T_2) - E(^2E)$, which in turn determines the ^2E and $^4T_2$ admixture coefficients.

These results show that the ionic radius of the modifier is important in determining the relative numbers of high-field and low-field sites, and hence the overall emission shape. Indeed the relative occupancy of low-field and high-field sites differs for the various glasses. For example, the strength of the ^2E emission relative to the rest of the emission is greater for ED-2 (which has Li^+ and Ca^{2+} modifiers) than for SLS7b/4 (which has K^+ and Pb^{2+} modifiers). The strength of ^2E emission for the ED-2 and SLS7b/4 glasses (figures 4 and 6) is an example of this effect. For SLS7b/4 and ED-2 glasses, which have Li^+ and K^+ modifiers, respectively (table 1), the relative amount of ^2E

emission as measured by the intensity ratio $R = I(^2E)/I(T_2)$ is greatest for ED-2 and smallest for SLS7b/4 (figures 4 and 6). That the ED-2 glass should provide the most tightly packed oxygen network and the potassium–lead glass (SLS7b/4) the most open structure and greatest number of low-field sites is in accord with the luminescence results.

4.4. Lifetime and time-resolved emission spectroscopy

The luminescence decay rate contains both temperature-dependent and temperature-independent terms, i.e.

$$1/\tau(T) = 1/\tau_s + (1/\tau_d)\coth(\hbar\omega/2kT) + (1/\tau_{NR})\exp(-\Delta E/kT) \qquad (5)$$

in which τ_s represents the radiative lifetime from magnetic dipole transitions or from electric dipole transitions induced by static odd-parity distortions. The second term, a dynamic contribution induced by odd-parity vibrations of effective frequency ω increases the decay rate (and hence emission intensity) with increasing temperature. The final term in equations (5) is associated with phonon-assisted non-radiative decay to the ground state for which the activation energy is ΔE. Other effects such as energy transfer and excited state absorption introduce temperature-independent decreases to the luminescence decay rate. The integrated intensities of the photoluminescence spectra are strongly dependent on temperature, being quenched at 300 K to 20% of their low-temperature value. Such changes are related to changes in the luminescence decay time. As a consequence of equation (5) the decrease in intensity at high temperatures is attributed to thermally activated non-radiative decay.

In these Cr^{3+}-doped glasses the photoluminescence after pulsed excitation decays on different time scales according to the spectral range detected. Although none of the decay patterns is exponential in time, the decay of the R line is most nearly so. These non-exponential decay patterns confirm the multi-site occupancy by Cr^{3+} ions in glasses and/or interactions between the optical centres (Huber 1984, Jonscher 1986). In the R-line region the initial decay times are about 100 ms, whereas at emission wavelengths in the $^4T_2 \rightarrow {}^4A_2$ broad band more rapid decay times of about 10 ms are observed. For the ED-2 glass, initial decay rates at 10 K ranged from 1.1×10^{-1} to 2.6×10^{-1} s^{-1} for the R line and from 2.3 to 11.1 ms^{-1} for the $^4T_2$–$^4A_2$ band. Similar results were obtained for each of the glasses. Because of the different time scales of the two emission processes it is possible to separate spectrally the $^2E \rightarrow {}^4A_2$ and $^4T_2 \rightarrow {}^4A_2$ emissions of the ED-2, G8035 and SLS7b/7 glasses. Time-resolved spectra for the ED-2 glass are shown in figure 7; note that the half-width of the R line is almost 200 cm^{-1}. The weak structure in the long-wavelength tail of the R line is its vibrational sideband. The R lines and their vibrational sidebands for ED-2, G8035 and SLS7b/7 glasses are almost identical, testifying to the extent of inhomogeneous broadening by disorder in each case.

4.5. Fluorescence line narrowing

The width of the R line in figures 4 and 7 and the non-exponential lifetime behaviour follows from Cr^{3+} ions occupying many sites with different crystal-field splittings. Averaging over the distribution of sites yields the inhomogeneously broadened R line. The R line of G8035 glass at $T = 4$ K excited at 655 nm is compared in figure 8 with its FLN component excited near the R-line peak (683.5 nm). Those R_1 and R_2 transitions resonant with the laser emit into the very narrow FLN line. The weaker component at longer wavelengths is associated with Cr^{3+} ions resonantly excited at the laser wavelength

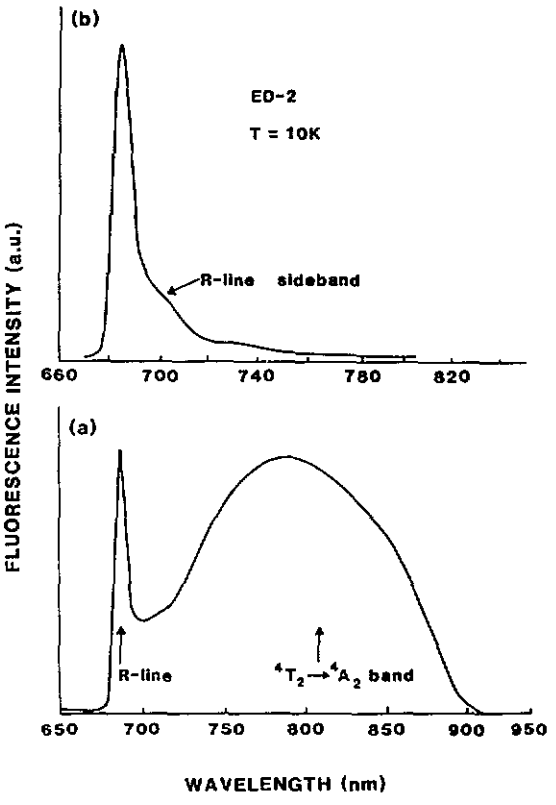

Figure 7. A comparison of the time-resolved R-line photoluminescence with the composite R-line–broad-band spectrum for ED-2 measured at 10 K.

decaying non-radiatively to the lower lying of the ^2E levels split by crystal-field distortion, which then emit in the R_1 line. At higher temperatures (e.g. $T = 77$ K) excitation at the same wavelength results in the appearance of the R_2 line due to thermal excitation to the higher-lying level of ions resonantly excited in the R_1 line. Thus at higher temperatures the FLN spectrum consists of the R_2 line of ions in high-field sites, an R_1 line due to ions in low-field sites, and the resonant FLN line. Figure 9 shows that the FLN R_1 and R_2 components for ED-2 glass at 77 K for various excitation wavelengths undergo linear shifts to longer wavelengths with increasing excitation wavelength. However, the R_1–R_2 splitting is larger for longer-wavelength excitation. Indeed the splitting for SLS7b/7 is 50 cm^{-1} at 678 nm and 56 cm^{-1} at 691.7 nm. Similar results are obtained for the ED-2 and G8035 glass; in the former case the splitting varies across the R line from 50 to 54 cm^{-1} and in the latter from 49 to 57 cm^{-1}, energy splittings very much larger than those observed by ESR studies of the ground state (section 4.1).

For free ions, the homogeneous width reflects lifetime broadening and $\Gamma_h \simeq \tau_R = A_{f0}^{-1}$. Vibrational modulation of the electronic energy levels provides an additional lifetime broadening in solids and produces 'vibronic' sidebands when the electron–vibrational coupling is strong. In crystals the vibrational spectrum may involve local modes and lattice phonons. Assuming a Debye spectrum of lattice phonons leads to a reasonable estimate of the homogeneous width of the R line in MgO and Al_2O and its temperature dependence (Henderson and Imbusch 1989, ch 5). The homogeneous width of the R line in glasses measured using FLN exceeds that in crystals by a factor of 20

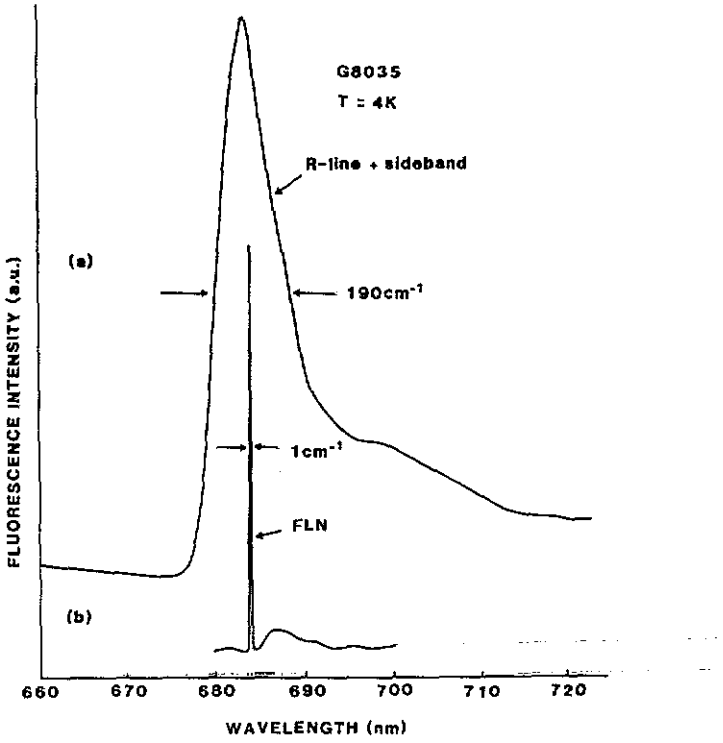

Figure 8. (*a*) The R-line and (*b*) resonant FLN spectra for G8035 measured at 4 K. The R_1 line is also observed in FLN displaced to a longer wavelength from the resonant FLN line.

or so, suggesting an additional source of broadening in glassy matrices. This excess homogeneous width for silicate glasses is symptomatic of disorder involving two-level vibrational systems (TLS) (Bergin *et al* 1986). The FLN broadening which can be followed up to about 120 K for the ED-2 glass was barely detectable above 70–80 K for G8035 and SLS7b/7 glasses. In other respects, however, the variations in the homogeneous width with temperature are quite similar: $\Gamma_h(T)$ varies linearly with temperature up to $T = 50$–60 K (figure 10) and quadratically with T above about 60 K owing to the onset of Raman relaxation. The densities of tunnelling modes for the TLS may be determined from the weak R-line sideband measured by excitation in the long-wavelength tail of the R line (figure 11). In glasses, where the orbit–lattice coupling involves local vibrations only, the amplitude model for the density $\rho(\omega)$ of vibrational states at angular frequency ω is appropriate and the sideband intensity $I(\omega)$ is

$$I(\omega) = C|\langle V\rangle|^2\rho(\omega)/\omega \tag{6}$$

where C is a constant and V an electronic sensitivity factor. The density of vibrational states, which scales as $\omega I(\omega)$, is also shown in figure 11. From the observed sideband intensity $I(\omega)$, and using the amplitude model the following approximate expressions hold:

$$\rho(\omega) = \begin{cases} \zeta\omega^2 \\ 2\zeta\omega_1^2 \end{cases} \quad \text{for} \begin{cases} 0 < \omega < 50\ \text{cm}^{-1} & (7) \\ 50\ \text{cm}^{-1} = \omega_1 < \omega < 350\ \text{cm}^{-1} & (8) \end{cases}$$

whereas for a Debye crystal $\rho(\omega) = \gamma\omega^2$ for $0 < \omega < 350\ \text{cm}^{-1}$. By comparison with the

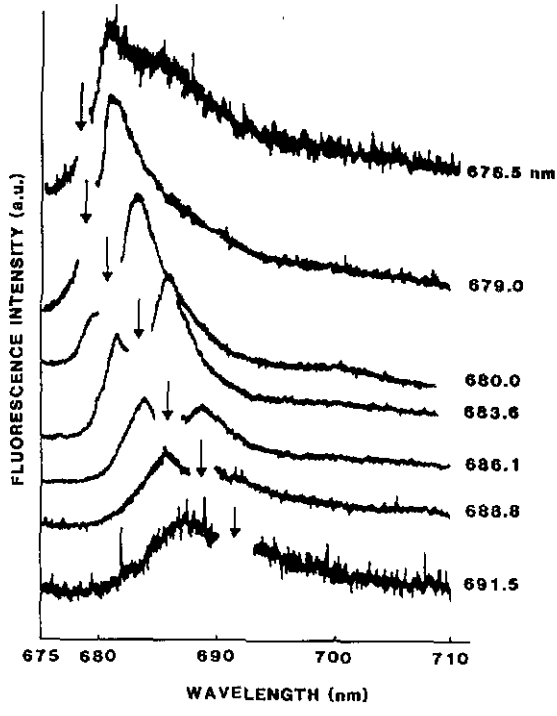

Figure 9. The R_1–R_2 splitting measured using FLN as a function of excitation wavelength for the ED-2 glass, measured at $T = 77$ K.

Debye crystal it is determined that $\zeta \simeq (50\text{–}60)\gamma$ for ED-2, G8035 and SLS7b/7 glasses. The ratios of the zero-phonon line to sideband intensities, i.e. the Huang–Rhys factors S are in the range 5–7 for glasses whereas $S \leqslant 1$ for crystals such as $Al_2O_3:Cr^{3+}$ (Henderson and Imbusch 1989, ch 5). A comparison of the experimental relative intensities for glass and crystal with that calculated using the amplitude and Debye model, respectively, for the density of states yields

$$|\langle V\rangle|^2\omega_1^2/|\langle V^1\rangle|^2 v^2 \simeq 0.6 \tag{9}$$

where v is the average velocity of sound in the crystal. This quantity may be used to determine the linewidth $\Gamma(T)$ of the FLN line for the glass relative to the crystal. For the glass and assuming Raman relaxation (Henderson and Imbusch 1989, ch 5),

$$\Gamma(T) = A\,\alpha|\langle V^1\rangle|^4 \int_0^\infty \frac{\omega^{-2}\rho(\omega)^2\exp(\hbar\omega/kT)}{[\exp(\hbar\omega/kT)-1]^2}\,\mathrm{d}\omega \tag{10}$$

whereas for the Debye crystal

$$\Gamma(T) = \frac{A\alpha^4|\langle V\rangle|^4\gamma^2}{v^4}\int^\infty \frac{\omega^6\exp(\hbar\omega/kt))}{[\exp(\hbar\omega/kT)-1]^2}\,\mathrm{d}\omega. \tag{11}$$

Evaluating the two integrals at (say) 80 K gives

$$[\Gamma(T)]_c/[\Gamma(T)]_g \simeq 0.21. \tag{12}$$

Since for ruby $\Gamma(80) \simeq 0.12\ \mathrm{cm}^{-1}$ and for the ED-2 glass $\Gamma(80) \simeq 3.6\ \mathrm{cm}^{-1}$ the exper-

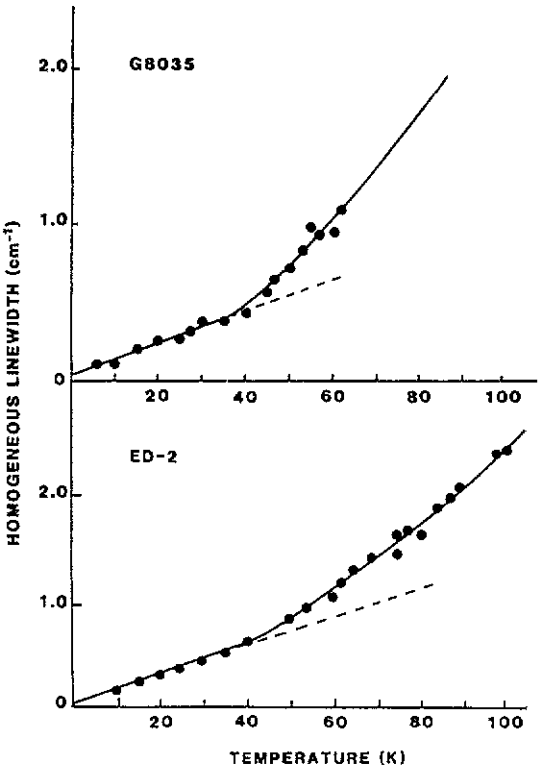

Figure 10. The temperature dependence of the homogeneous width $\Gamma_h(T)$ for G8035 and ED-2 glasses.

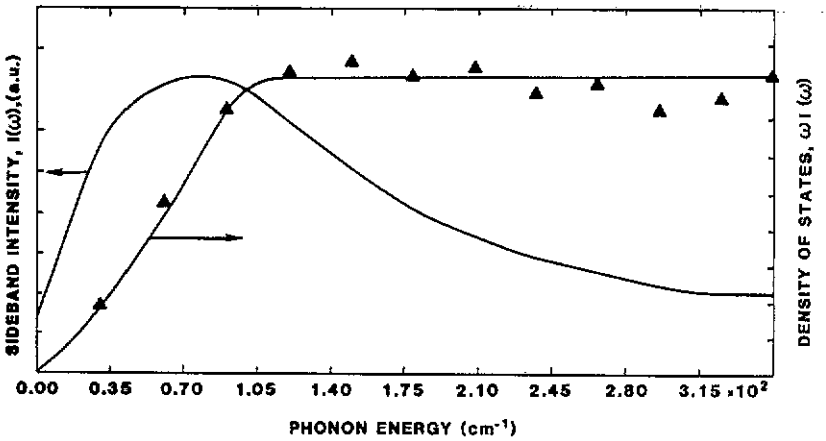

Figure 11. The density $\omega I(\omega)$ of vibrational states and the luminescence intensity $I(\omega)$ of the R-line sideband for the Cr^{3+}-doped SLS7b/7 glass.

imental value of this ratio is 0.33. In view of the simplifying assumptions made in this analysis the accord between experiment and theory is regarded as satisfactory.

5. Conclusions

In comparison with crystalline solids both R-line and broad-band spectra are broadened in glasses, because of the multiple crystal-field sites available in glasses for the Cr^{3+} ions, where the crystal-field splittings are slightly different. Such inhomogeneous broadening is revealed in measurements of the spectral profile during laser excitation, whence the peak position and shape of the emission spectra are observed to vary with laser excitation wavelength. A further consequence of the multi-site occupancy by Cr^{3+} ions is the dependence of the luminescence lifetime on the emission wavelength, with consequent multi-component decay patterns following pulsed excitation. It is the multi-component decay which makes it possible to time-resolve the Cr^{3+} emission into its components. The integrated intensity of the Cr^{3+} fluorescence decreases with increasing temperature until at room temperature it is only 20–30% of the value at 10 K. The reduced efficiencies at high temperatures are due to luminescence quenching via the overlap of the $^4T_2$ and $^4A_2$ configurational coordinate curves. The activation energy for this process depends on the energy of the $^4T_2$ level being less for low-field sites; there are more low-field sites in SLS7b/4 than in the other silicate glases. Similar results were reported in fluoride glasses by Hollis *et al* (1987). The non-exponential decay for both ^2E and $^4T_2$ transitions and the observed lifetime variations of different centres may be accounted for by random distributions of site distortions or by ion–ion coupling between Cr^{3+} ions randomly distributed in glasses. Various workers have found that Cr^{3+}-doped glasses containing Li^+ and Ca^{2+} modifiers have the highest luminescence quantum efficiencies (Andrews *et al* 1981, Reisfeld 1987, Van Die *et al* 1988, Seelet 1987, Sarkies 1990, Webb 1990). Furthermore, as the molar percentage of silica is increased, the quantum efficiency of the Cr^{3+} luminescence falls. Although not expected from the molar composition and doping levels alone, this behaviour follows from clustering of the Cr^{3+} as the fraction of network reacted with the modifier ions is reduced. These data are in accord with Lacy's (1955) discussion of structural compaction or distension by modifiers, a looser structure providing the possibility of vibrationally assisted non-radiative decay of Cr^{3+} ions in low ligand fields. One might expect that, since many Cr^{3+}-activated laser crystals (e.g. $BeAl_2O_4:Cr^{3+}$) contain rings, the glasses with a higher silica content would give higher quench temperatures and quantum efficiencies for the fluorescence. As Imbusch *et al* (1990) point out, the dominant components come from the magnitude and symmetry of the interactions of the dopant ions with nearest-neighbour ligand ions. A high ligand field at the dopant, the absence of clustering of dopant ions, and octahedral coordination with low distortion of nearest neighbours to the dopant ion are the most important requirements. The coordination symmetry further away from the optical centre is unimportant, as is exemplified in many Cr^{3+}-doped crystals.

The narrowness of the FLN R line is dramatic evidence of the inhomogeneous broadening due to static crystal-field disorder. Each Cr^{3+} ion experiences a slightly different crystal field owing to the average positions of neighbouring ligand ions. The results for all three glasses are quite similar and follow the trends reported earlier by Bergin *et al* (1986) for the ED-2 glass. At temperatures below 50–60 K, $\Gamma(T)$ varies as the absolute temperature whereas at higher temperatures the variation is quadratic in T. The transition from T to T^2 behaviour occurs at slightly different temperatures for the different glasses. The linear dependence on T at low temperatures results from optical dephasing

due to electric dipole–dipole interactions between Cr^{3+} ions and tunnelling modes of the two level vibrational systems. Such tunnelling modes have a high density of states and low frequency. In consequence their amplitude even at low temperatures contributes significantly to the homogeneous linewidth. At higher temperatures ($T > 50$–60 K) the quadratic dependence of $\Gamma(T)$ on temperature is consistent with a two-phonon Raman relaxation process (Bergin *et al* 1986, Henderson and Imbusch 1989, ch 5).

Acknowledgments

At Strathclyde this work has been supported by a research grant (GR/E/32549) from the Science and Engineering Research Council. The glasses SLS7b/4 and SLS7b/7 were prepared by DBH at the University of Sheffield, where the work was supported by a research contract (RU 10/40) from the Procurement Division of the Ministry of Defence.

References

Andrews L J, Lempicki A and McCallum B C 1981 *J. Chem. Phys.* **74** 5526–38
Balta P and Balta E 1976 *Introduction to the Physical Chemistry of the Vitreous State* (Tunbridge Wells, Kent: Abacus) ch 3, pp 59–187, ch 4, pp 129–87
Barrer R M and Vaughan D E W 1967 *Trans. Faraday Soc.* **63** 2275
Bergin F, Donegan J F, Glynn T J and Imbusch G F 1986 *J. Lumin.* **34** 307
Boulon G, Garapon C and Monteil A 1988 *Excited States of Transition Metal Ions* ed M Jezowska-Trzebiatowska, J Legendziewicz and W Strek (Singapore: World Scientific) p 96
Engstrom H and Mollenauer L F 1973 *Phys. Rev.* B **7** 1616
Healy S M, Donnelly C J, Glynn T J, Imbusch G F and Morgan G P 1989 *J. Lumin.* **44** 65
Henderson B and Hall T P P 1967 *Proc. Phys. Soc.* **90** 511
Henderson B and Imbusch G F 1989 *Optical Properties of Inorganic Solids* (Oxford: Oxford University Press)
Henderson B and Wertz J E 1978 *Defects in the Alkaline Earth Oxides* (London: Taylor & Francis) p 36 et seq
Hollis D B, Parke S and Payne M J P 1987 *Tunable Solid State Lasers II (Springer Series in Optical Science 52)* ed L G de Shazer, A B Budgor and A Pinto) (Berlin: Springer) p 53
Howitt D G and McElfresh D K 1982 *Phys. Chem. Glasses* **23** 107–9
Huber D L 1984 *Coherence and Energy Transfer in Glasses* ed P A Fleury and B Golding (New York: Plenum) p 125
Imbusch G F, Glynn T J and Morgan G P 1990 *J. Lumin.* **45** 63
Jonscher A K 1986 *Structure and Bonding in Non-Crystalline Solids* ed G E Walrafen and A G Reversz (New York: Plenum) p 101
Kushida T and Takushi E 1975 *Phys. Rev.* B **12** 824
Lacy E D 1955 *The Vitreous State* (Sheffield: Glass Delegacy of University of Sheffield) p 23
Marshall A, O'Donnell K P, Yamaga M, Henderson B and Cockayne B 1990 *Appl. Phys.* A **50** 565
Mitra S K and Hockney R W 1980 *J. Phys. C: Solid State Phys.* **13** L739
Monteil A, Garapon C and Boulon G 1988 *J. Electrochem. Soc.* **88** 24
Paul A 1982 *Chemistry of Glasses* (London: Chapman and Hall) p 51
Reisfeld R 1987 *Spectroscopy of Solid State Laser-type Materials* ed B Di Bartolo (New York: Plenum) p 343
Sarkies P H 1990 *PhD Thesis* University of Sheffield
Seelet W R 1987 *PhD Thesis* University of Oldenburg
Shackelford J F and Masaryk J S 1978 *J. Non-Cryst. Solids* **30** 127
Shelby J E 1979 *Treatise Mater. Sci. Technol.* **17** 1
Siefert F A, Mysen B O and Virgo D 1983 *Phys. Chem. Glasses* **24** 141
Struve B and Huber G 1985 *Appl. Phys.* B **57** 45
Sugano S, Tanabe Y and Kamimura H 1970 *Multiplets of Transition-Metal Ions in Crystals* (New York: Academic)
Van Die A, Leenaers A C H I, Blasse G and Van der Weg W F 1988 *J. Non-Cryst. Solids* **99** 32
Webb R S 1990 *PhD Thesis* University of Sheffield
Yamaga M, Henderson B and O'Donnell K P 1989 *J. Phys. Condens. Mater* **1** 9175
Yamaga M, Henderson B, O'Donnell K P, Trager-Cowan C and Marshall A 1990 *Appl. Phys.* B **50** 425
Yang N and Chen X 1989 *J. Chinese Ceram. Soc.* **17** 165